

High Gain Compact Dual Band Reconfigurable Antenna Using Multilayer FSS for WLAN and RADAR Applications

Rashmi A. Pandhare^{1, *}, Mahesh P. Abegaonkar², and Chandresh Dhote¹

Abstract—This paper presents the design of a frequency reconfigurable monopole microstrip patch antenna for wireless communication applications. The proposed antenna functions in one single-band mode and one dual-band mode, depending on the diode switching configuration. When the diode is in the OFF state, the proposed antenna operates at single band 5.8 GHz (WLAN), and in the ON state, the antenna operates at dual bands 1.8 GHz (GPS/RADAR) and 5.2 GHz (WLAN). To enhance the gain of the proposed reconfigurable antenna, a multilayer frequency selective surface (FSS) reflector is presented. A significant enhancement in gain has been achieved in a low-profile design. The average peak gain of the antenna has been increased from 4 dBi to 6 dBi as a consequence of the use of the FSS reflector. The simulation of the proposed design is carried out using CST (Computer Simulation Technology) based on the FIT (Finite Integration Technique) numerical method. To validate the simulated results, a prototype of the antenna was fabricated and measured using PIN diodes. The simulated and measured results of the proposed antenna exhibit a reasonable agreement.

1. INTRODUCTION

The need for portable electronic devices that operate at several frequency bands has increased as a result of the lightning-fast advancements in electronics and wireless communications for a variety of applications. Multi-band and reconfigurable antennas are a requirement for modern communication equipment. Reconfigurable antennas have attracted a significant amount of attention due to their applicability in modern mobile communication services. Different switching techniques, such as varactor diodes, lumped elements, optical switches, PIN diodes, and micro-electro-mechanical systems (MEMS), can be used to accomplish reconfigurability operations in today's wireless communication devices operating in a variety of frequency bands. However, compared to PIN diodes, MEMS switches have higher costs and lower reliability [1, 2]. Various beneficial forms have been suggested in the past for building multiband antennas. In [3], a 9-shaped frequency reconfigurable antenna is presented. In [4], a dual band T-shaped antenna is discussed. A slotted L-shaped frequency and pattern reconfigurable antenna for (WiMAX/WLAN) applications is reported in [5]. However, the gains of only 0.5 dB and 2 dB are obtained at 3.550 GHz and 5.775 GHz, respectively. [6] describes a multi-band inverted-F frequency reconfigurable antenna that has an average gain of less than 4.5 dB. [7] introduces an F-shaped frequency reconfigurable antenna with a gain of no more than 2.5 dBi. A B-shape antenna is proposed in [8]. In [9], a dual-band E-shape monopole antenna is presented for Wireless-Area-Network (WLAN) applications with a gain of no more than 4.3 dB. An F-shape dual-band antenna for RFID and WLAN applications is discussed in [10]. A C-shaped monopole antenna, obtaining impedance bandwidths of 2.39–2.52 and 5.12–7.12 GHz with the measured gains of 2.0 and 3.1 dBi, is presented in [11]. An H-shaped antenna for GPS and Wi-Fi applications with a gain of less than 3.7 dBi is proposed in [12]. A dual-band frequency

Received 4 June 2022, Accepted 30 August 2022, Scheduled 2 March 2023

* Corresponding author: Rashmi A. Pandhare (rush9ap@gmail.com).

¹ Department of Electronics & Communication Engineering, Indian Institute of Information Technology, Nagpur, India. ² Center for Applied Research in Electronics, Indian Institute of Technology, New Delhi, India.

reconfigurable patch antenna designed to cover WLAN bands at 2 GHz and a second band ranging from 5.3 GHz to 5.8 GHz using two varactor diodes is reported in [13]. In [14], a new miniaturised switchable-band microstrip patch antenna array using eight PIN-diodes is presented for WLAN and Worldwide Interoperability for Microwave Access (WiMAX) applications. A triband slot antenna designed to cover bands of 2.4 GHz, 5 GHz, and 3.5 GHz for WLAN and WiMAX applications using two PIN diodes is reported in [15], where the gain is less than 5 dBi for all operating frequencies. [16] describes a quad-band frequency tunable antenna for 5G sub-6 GHz applications using three PIN diodes. This antenna covers 3.31–6.03 GHz in sensing mode and three bands in communication mode: 3.31–4.32, 3.78–4.98, and 4.98–5.96 GHz. However, the gain is not more than 2.3 dBi. Although several switching approaches and unique concepts have been used to make the antenna’s multiband frequency reconfigurable operations possible, the employment of switching elements in the design increases the design’s complexity and reflection loss, which lowers the antenna’s gain and bandwidth. However, improvements in modern wireless communication demand high-performance antenna radiators in terms of bandwidth and gain, as well as the ability to operate in a reconfigurable manner [17].

The need for a single antenna that can handle various standards while using the fewest possible diodes has significantly increased in recent years. For contemporary wireless applications, this article suggests a high gain dual band reconfigurable antenna in order to offer the general public cutting-edge on-demand services. The single antenna is suitable for GPS/RADAR and WLAN applications since it functions in two states using RF PIN diodes. One PIN diode has been placed on the slotted patch structure to achieve the desired state of frequency bands. Using a multilayer frequency selective surface (FSS) reflector, the suggested reconfigurable antenna’s gain is increased. The FSSs are positioned below the antenna to serve as a reflector and increase gain for all operational modes. The proposed antenna is designed and investigated using the CST-EM software package in terms of the antenna’s different parameters including impedance bandwidth characteristics, radiation patterns, and antenna gain evaluation. In this manuscript, a compact monopole antenna is presented which radiates at single and dual frequency bands, including GPS and WLAN. The antenna consists of one lumped element (RLC [resistance, inductance, and capacitance]) switches for reconfigurability operation, and to integrate a PIN diode switch, a slot of 1.25 mm is reserved in the initial design.

2. ANTENNA DESIGN CONFIGURATION

The proposed antenna configuration is shown in Fig. 1. The radiating element patch and ground plane are printed on a 1.6 mm thicker lossy substrate FR-4 (having a dielectric constant of 4.3 and a loss tangent of 0.025). The overall dimensions of the proposed antenna are $W_s = 30$ mm, $L_s = 42$ mm, and $H = 1.6$ mm. The effective lengths of the patch are $L_1 = 22$ mm, $L_2 = 14$ mm, and $L_3 = 9.6$ mm. The patch is printed on the top of the substrate material, and the ground plane, with the dimension of $W_g = 30$ mm and $L_g = 13.8$ mm, is printed on the back of the substrate. The proposed antenna is excited using a $50\ \Omega$ microstrip feed line having a 3.8 mm width. The waveguide port or connector is assigned to the microstrip line to excite the antenna. In order to integrate the lumped element switch, the 1.25 mm slot is reserved in the radiating element. Table 1 summarizes the details of the proposed antenna’s various design parameters.

Table 1. Design parameters of the proposed antenna.

Parameters	Dimensions (mm)	Parameters	Dimensions (mm)
W_s	30	W_g	30
L_s	42	L_g	13.8
W_1 & W_2	3.8	L_2	14
L_1	22	L_3	9.6

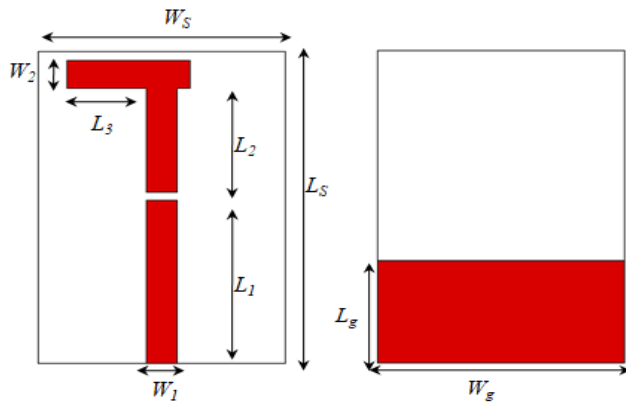


Figure 1. Proposed antenna and ground plane.

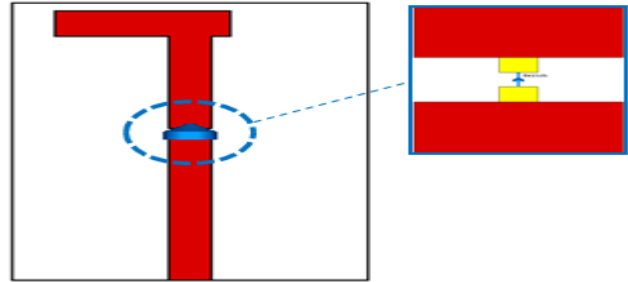


Figure 2. Proposed antenna and ground plane.

3. RECONFIGURABLE ANTENNA DESIGN

An antenna's basic structure can be reconfigured to achieve other frequency bands by using a PIN diode acting like a variable resistor in the RF (Radio Frequency) range, as shown in Fig. 2.

In the basic structure of a proposed monopole antenna, the effective lengths of the patch are $L_1 = 22$ mm, $L_2 = 14$ mm, and $L_3 = 9.6$ mm. The patch is printed on the top of the substrate material. The longer length of the patch will make the antenna resonate in the lower band, and the shorter length of the patch will make the antenna resonate in the higher band. As shown in Fig. 2, the PIN diode is inserted into the reserved 1.25 mm slot in the radiating element. The PIN diode provides an open and short circuit in its ON and OFF conditions, respectively. The presence of a PIN diode increased the overall length of the patch, and the antenna started resonating at a lower frequency. However, the absence of the PIN diode shorted the length of the patch, and the antenna started resonating at a higher frequency. In STATE-I, Diode 'D' is in OFF condition, then the antenna operates at 5.8 GHz with a maximum peak gain of 2.2 dBi. In STATE-II, the antenna resonates at dual band frequencies of 1.8 and 5.2 GHz with peak gain values of 1.4 and 3.3 dBi, respectively. The reflection coefficient plots for both the states of the diode switching configuration are illustrated in Figs. 3(a) and (b), respectively.

To implement the electronic reconfigurable switching operation in the simulation, an initially ideal PEC strip (0.2×0.4 mm²) was used as a switching element, and each perfect electric conductor (PEC) strip was replaced by an RF PIN diode in practical conditions. The PIN diode model of MACOM part number MA4SPS402 has been used in the proposed antenna for switching purposes. According to the datasheet of the model, it consists of a lower parasitic inductance of 0.45 nH and an excellent RC constant (0.23 pS) [18]. But these nonsymmetrical configurations make the radiation patterns not very similar to omnidirectional radiation. Fig. 4 illustrates the 3D radiation patterns for single band (5.8 GHz) and dual bands (1.8 GHz and 5.2 GHz).

Figures 5(a) and (b) show the peak gain 1D plot of the proposed antenna for both states, revealing 2.2 dBi peak gain at single band 5.8 GHz and 1.4 dBi and 3.3 dBi peak gain at dual bands 1.8 GHz and 5.2 GHz, respectively.

4. FSS DESIGN CONFIGURATION

To improve the antenna performance, an FSS array has been incorporated as a reflector behind the antenna. Figs. 6(a) and (b) show the unit cell elements of FSS's layer-1 (square loop) and layer-2 (double square loop), constructed on the FR-4 dielectric material having relative permittivity (ϵ_r) = 4.3 and loss tangent ($\tan \delta$) = 0.025. Both the FSS unit cells of layer 1 and layer 2 have an overall size $22 \times 22 \times 1.6$ mm³ with an inner dimension (L_1) of 19 mm. The outer dimensions (w_1), inner dimension (w_2), and width (s) of the inner loop of layer-2 (second square loop) are 13.5 mm, 11 mm, and 1.25 mm. Initially, the layer-1 (square loop) type unit cell element is simulated by applying the Floquet mode

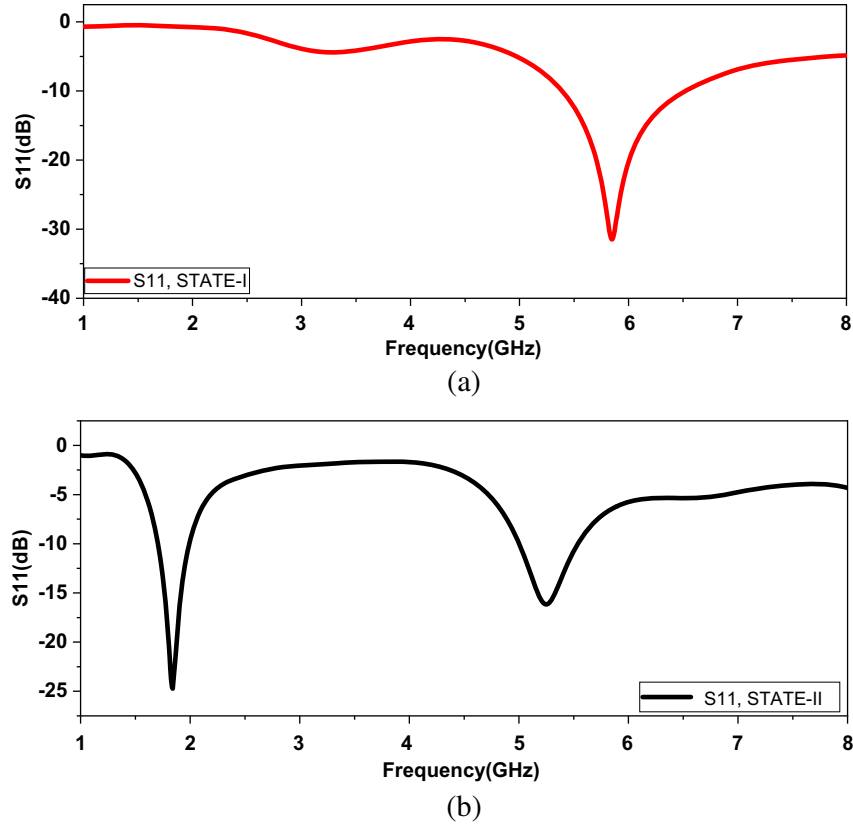


Figure 3. Reflection coefficient (S_{11}) plot of (a) single band operation STATE-I and (b) dual band operation STATE-II.

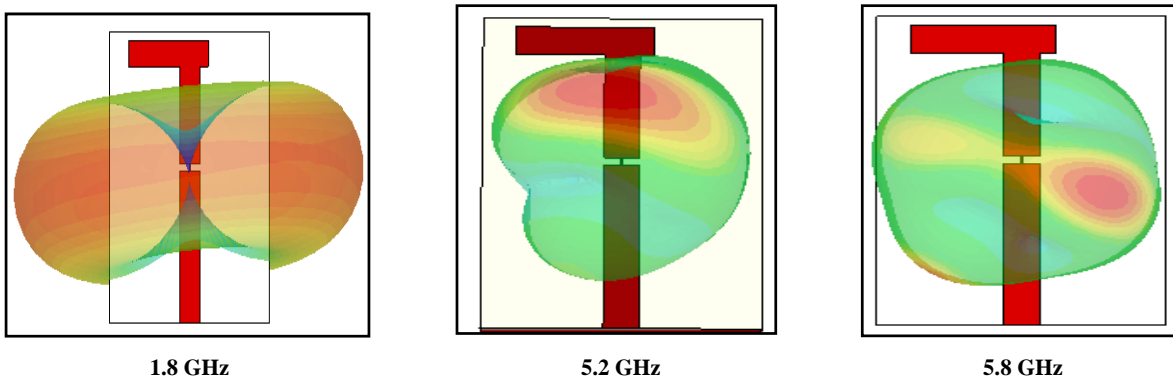


Figure 4. 3D farfield radiation patterns at 1.8 GHz, 5.2 GHz and 5.8 GHz.

port using the Finite Element Method (FEM) and achieving the single band 1.8 GHz frequency. Layer-2 (double square loop) has the same outer dimension as layer-1, which operates at dual bands of 1.8 and 5.5 GHz frequencies. The square loop FSS array and double square loop FSS array are cascaded at a gap of 2.8 mm. Layer-1 (square loop) and layer-2 (double square loop) design parameters are shown in Table 2.

The theory of transmission lines supports the development of an equivalent circuit model of FSS using inductive (L) and capacitive (C) lumped components. An equivalent circuit of FSS representing an infinite array of conducting strips, developed by Marcuvitz [19] allows the computation of inductive

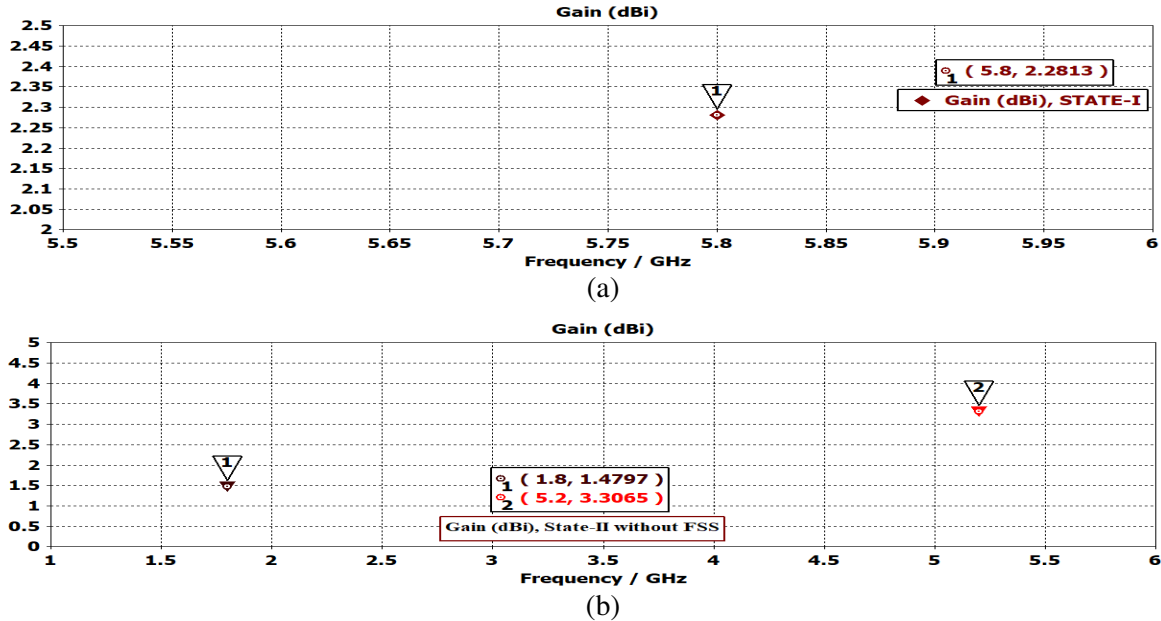


Figure 5. Gain vs frequency plot, (a) single bands-state I, (b) dual band-state II.

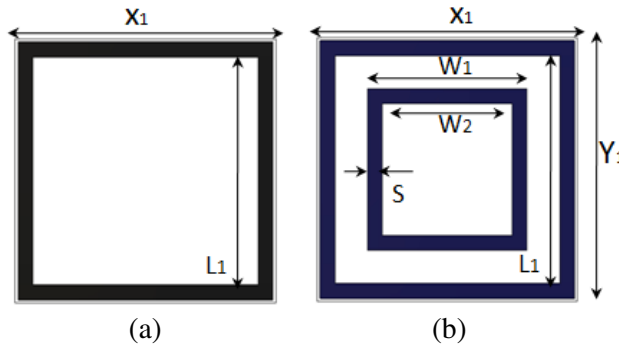


Figure 6. (a) Unit cell FSS of layer 1. (b) Unit cell FSS of layer 2.

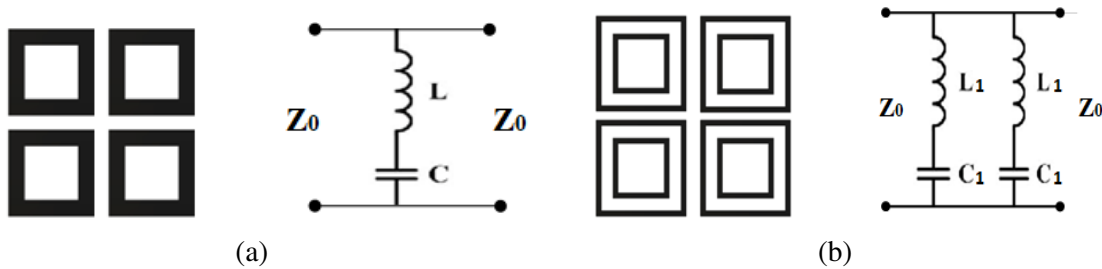


Figure 7. (a) Equivalent circuit unit cell FSS layer 1. (b) Equivalent circuit unit cell FSS layer 2.

(L) and capacitive (C) values.

The square loop and double square loop arrays with their equivalent circuit models are shown in Figs. 7(a) and (b), respectively. The square loop FSS represents the vertical and horizontal metal strips. The vertical metal strip acts as an inductive reactance and the horizontal strips as a capacitive reactance [20, 21]. Figs. 8(a) and (b) represent the arrays of FSS layer-1 (square loop) and FSS layer-2 (double square loop).

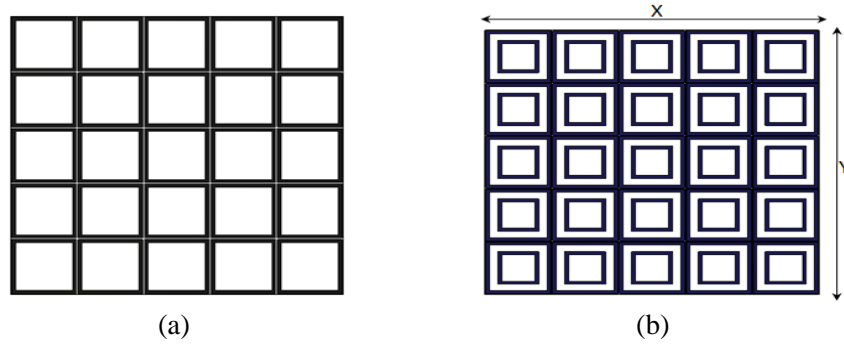


Figure 8. (a) Array of unit cell FSS layer 1. (b) Array of unit cell FSS layer 2.

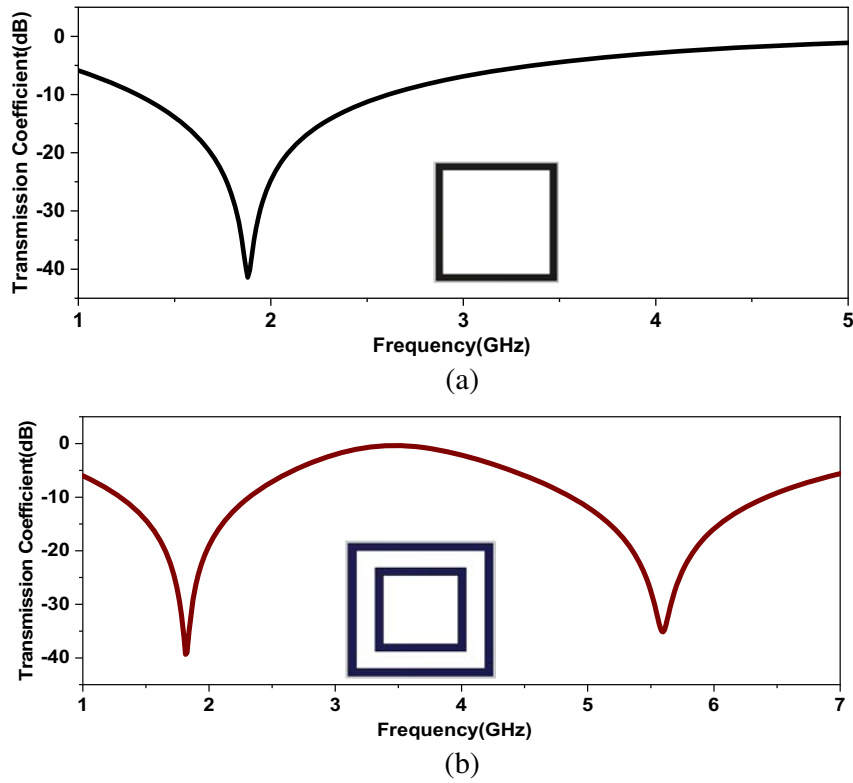


Figure 9. Transmission characteristics of proposed FSS. (a) Layer-1 (square loop). (b) Layer-2 (double square loop).

Table 2. Design parameters of layer-1 and layer-2.

Parameters	Dimensions (mm)
X_1 & Y_1	22
L_1	19
W_1	13.5
W_2	11
S	1.25
X & Y	110

Figures 9(a) and (b) represent the plots of transmission coefficient for unit cell FSS layer-1 (square loop) and layer-2 (double square loop). The square loop FSS layer-1 operates at the 1.8 GHz single frequency band while the double square loop FSS layer-2 covers the dual bands of 1.8 GHz (1.2–2.3 GHz) and 5.6 GHz (4.8–6.4 GHz).

Figure 10 represents the reflection phase of the FSS. It can be observed that the reflection phase decreases as frequency increases, and the zero phase reflection frequency is at 5 GHz, which is an essential condition to calculate the height of the FSS when it is used as a reflector below the antenna.

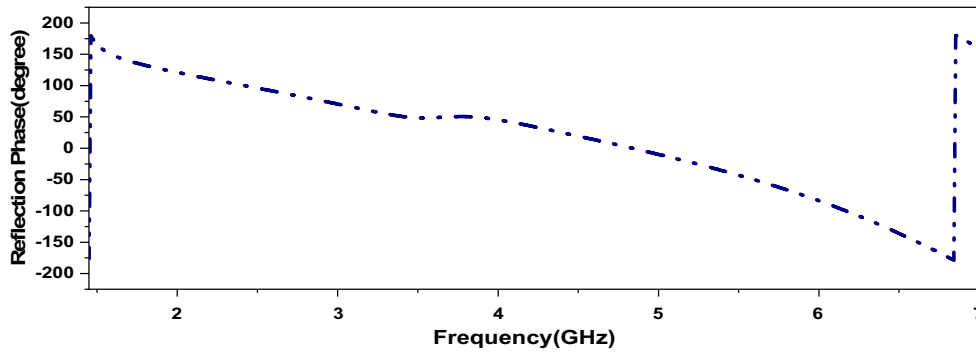


Figure 10. Reflection phase (in degree) of the FSS.

5. ANTENNA INTEGRATED WITH FSS

Figures 11(a) represents the unit cells of FSS layer-1 (square loop) and FSS layer-2 (double square loop) which are cascaded, and Figures 11(b) shows the representation of cascaded unit cell boundary conditions with Floquet mode ports. The 5 × 5 element FSS array is incorporated below the antenna to achieve the gain enhancement. Figures 12(a) and (b) show the front and side views of an antenna with a double-layer FSS array.

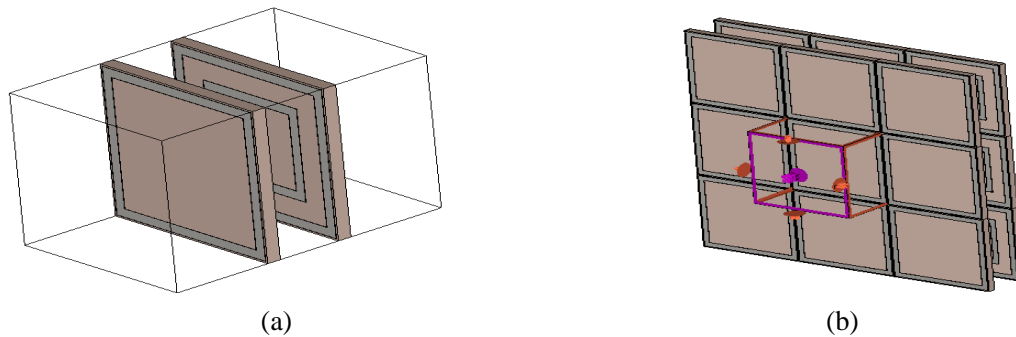


Figure 11. (a) Cascaded form of two unit cell FSSs. (b) Unit cell FSSs with unit cell boundary condition.

To achieve the gain increment, the location of the FSS behind the antenna is selected in such a way so that the radiated wave from the antenna and the reflected wave from the FSS are in phase. Therefore, the condition for the radiated wave and reflected wave to be in phase is given by [22, 23].

$$\phi_{\text{FSS}} - 2\beta h_1 = 2n\pi, \quad n = -1, 0, 1, 2 \tag{1}$$

Here, ϕ_{FSS} is the FSS reflection phase, β the free space propagation constant ($\beta = 2\pi/\lambda$), and h the the optimal height between antenna and FSS. From Fig. 10, the zero degree reflection phase frequency is found to be 4.9 GHz. Hence, the optimal height is calculated between FSS and the antenna, and it is found to be $h_1 = 24$ mm. The optimized height between the two FSS layers is $h_2 = 2.8$ mm.

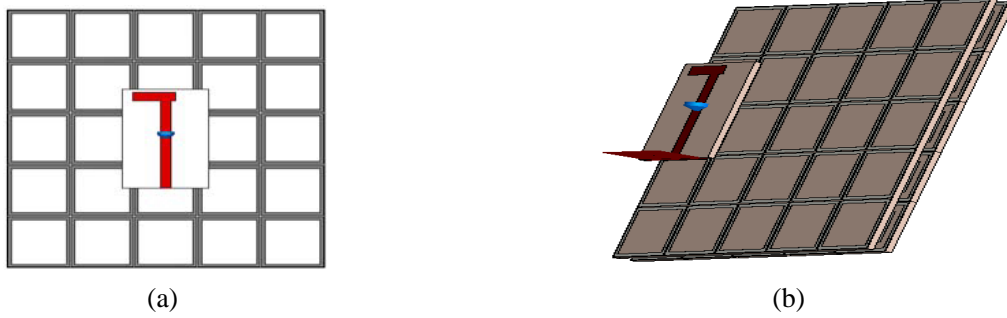


Figure 12. (a) Top view of antenna integrated with FSS. (b) Tilted side view of antenna with double layer FSSs.

Figure 13 shows the side view of the FSS placed at $h_1 = 24$ mm, behind the antenna. Figs. 14(a) and (b) show a comparison plot of the reflection coefficient (S_{11}) of an antenna with and without FSS for STATES I and II, respectively. It can be observed that the impedance bandwidth remains almost the same in both states after the application of the FSS reflector.

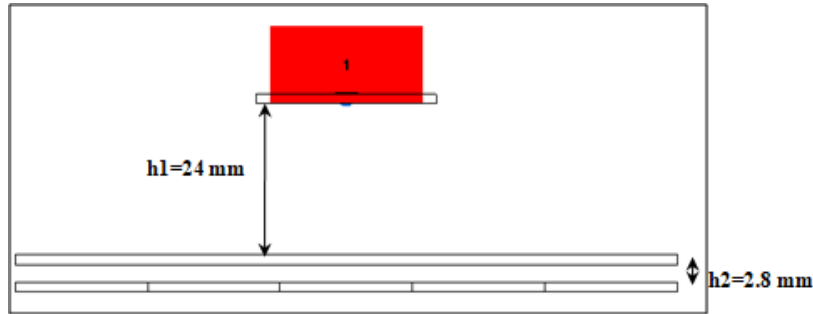


Figure 13. Side view of FSS place behind antenna.

Figures 15(a) and (b) show the comparison gain vs frequency 1D plots of antennas with and without FSS in both the STATES (I & II). In STATE-I, the antenna alone operates at 5.8 GHz with a peak gain of 2.2 dBi, and after the integration of FSS, it can be seen that there is an excellent gain enhancement of 5.8 dB. Similarly, in STATE-II, the antenna achieves the dual frequency bands with corresponding peak gains of 1.4 and 3.3 dBi. After the integration of FSS as a reflector behind the antenna, the achieved gains with corresponding frequencies are 7.3 and 6.8 dBi.

Table 3 shows how the reflection coefficient and peak gain operate with and without FSS. It has been noted that using the FSS reflector has caused the antenna's average peak gain to increase from 4 dBi to 6 dBi.

Table 3. Comparison of S_{11} and gain of all frequency bands with and without FSS.

STATES	Diode (D) Configuration	Frequency Bands (GHz)		Peak Gain (dBi)	
		Without FSS	With FSS	Without FSS	With FSS
I	OFF	5.8 GHz	5.8 GHz	2.2 dBi	5.9 dBi
II	ON	1.8 GHz, 5.2 GHz	1.8 GHz, 5.2 GHz	1.4, 3.3 dBi	7.3, 6.8 dBi

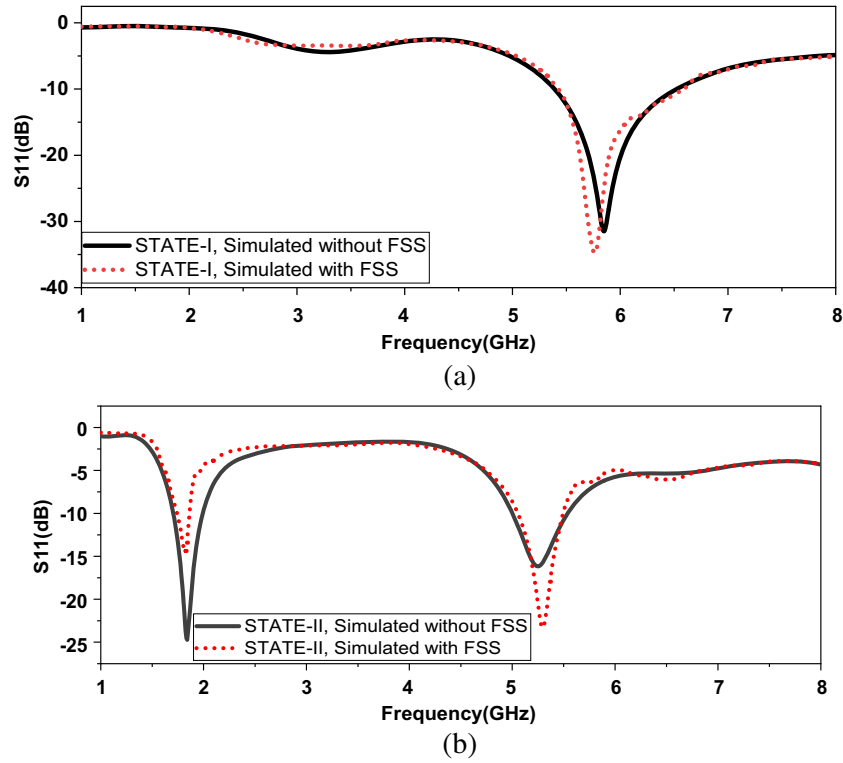


Figure 14. (a) & (b) Reflection coefficient (S_{11}) comparison plot of antenna with and without FSS for both the STATES (I & II).

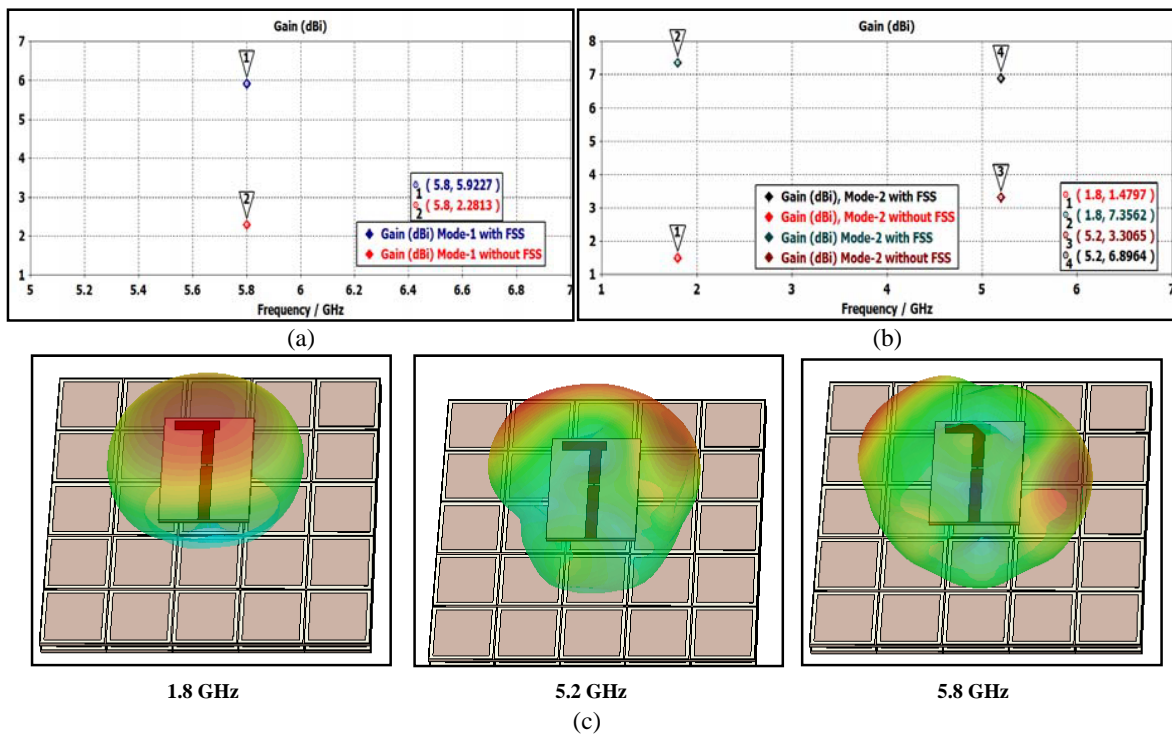


Figure 15. (a) Peak gain of antenna with and without FSS for STATE-I, (b) STATE-II respectively, (c) 3D radiation farfield pattern of antenna with FSS.

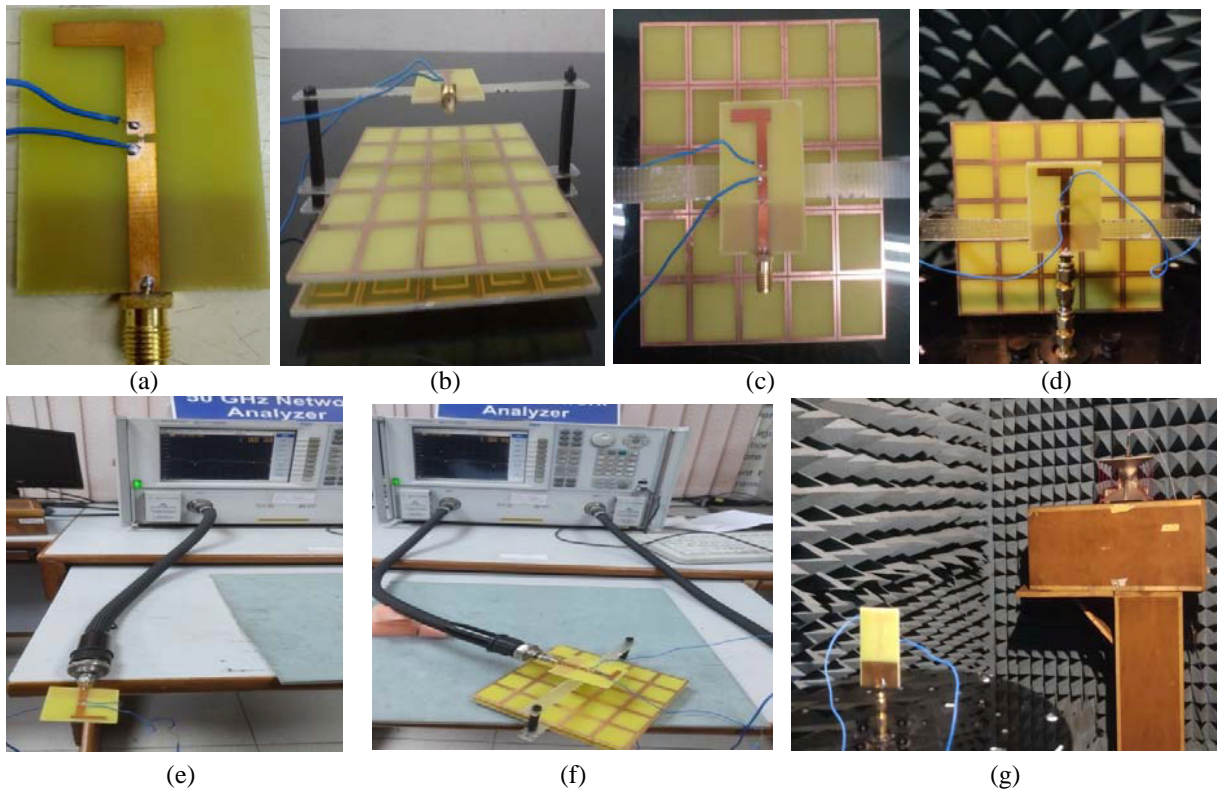


Figure 16. Fabrication and measurement setup of proposed antenna assembled with FSS, (a) antenna top view, (b), (c) side view and front view of antenna with double layer FSS respectively, (d), (g) radiation pattern measurement inside the anechoic chamber of antenna with and without FSS respectively, (e), (f) S_{11} measurement of antenna alone and with FSS using VNA.

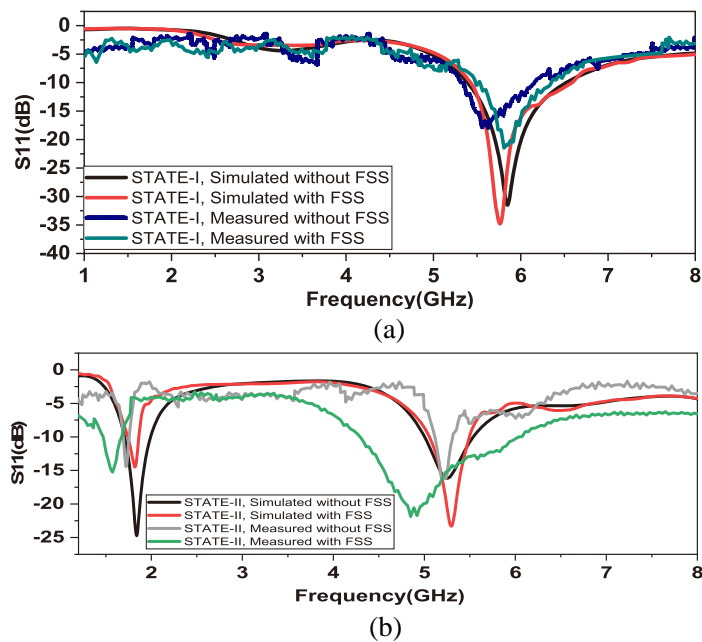


Figure 17. (a) Comparison of simulated and measured reflection coefficients (S_{11}) with and without FSS STATE-I, (b) STATE-II.

6. MEASUREMENT TEST SETUP & RESULTS DISCUSSION

The proposed antenna has been modelled and designed using 3D Electromagnetic Software, CST, based on Finite Integration Technique (FIT) and then fabricated. Fig. 16 depicts the antenna prototype fabricated model and the measurement test setup for the fabricated prototype antenna assembled with FSS. The reflection coefficient (S_{11}) is tested using the Keysight Vector Network Analyzer (N9918A), and the radiation patterns have been measured inside an in-house anechoic chamber with an Antenna Measurement Systems.

6.1. Reflection Coefficient (S_{11}) Characteristics

A comparison of the simulated and measured reflection coefficients (S_{11}) of the proposed antenna with and without FSS for both the STATES (I & II) is shown in Figs. 17(a) and (b), respectively. It can be observed that there is a good agreement between the simulated and measured results for both the switching configuration states. The slight difference occurs due to the fabrication tolerance, assembly error, and switching wires.

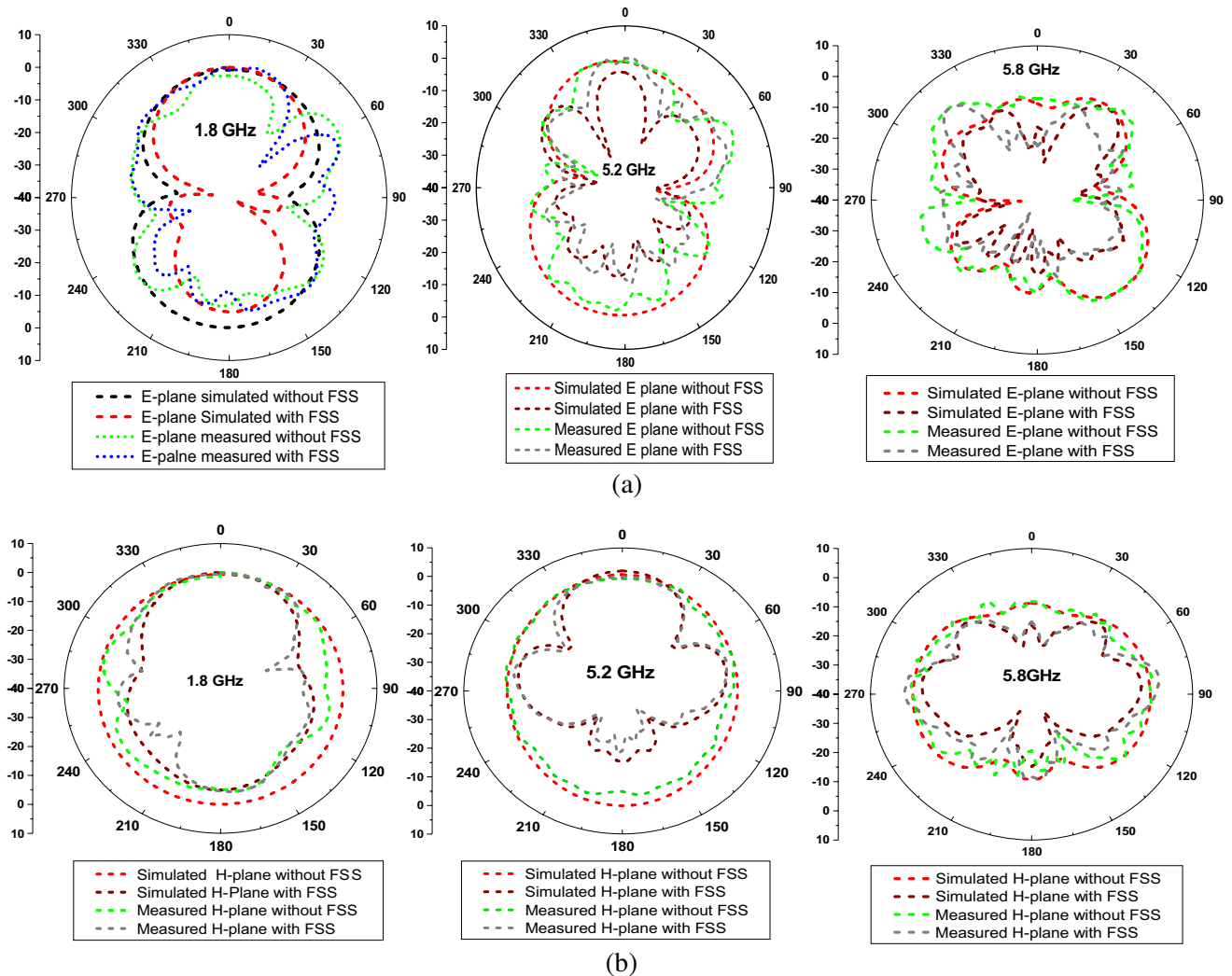


Figure 18. Comparison plot of simulated radiation patterns (E -plane and H -plane) of antenna with and without FSS at different frequencies 1.8 GHz, 5.2 GHz, 5.8 GHz, (a) E -plane, (b) H -plane.

6.2. Radiation Patterns

The simulated radiation patterns in the E and H planes of the proposed wideband antenna with and without FSS at 1.8 GHz, 5.2 GHz, and 5.8 GHz are shown in Fig. 18. It can be noticed that the antenna alone has almost stable radiation patterns which shows omnidirectional characteristics in the H (X - Z)-plane ($\phi = 0^\circ$) and bidirectional ones in the E (Y - Z)-plane ($\phi = 90^\circ$) over all bands. At higher frequencies, the antenna with FSS shows undesirable side lobes with the main lobe due to higher-order modes excitation and suppresses the back lobes due to the FSS reflector.

6.3. Gain versus Elevation Angle

Figure 19 shows the gain versus elevation angle theta (Degree) with constant azimuth angle ($\phi = 90$ Degree) for both states of PIN diode.

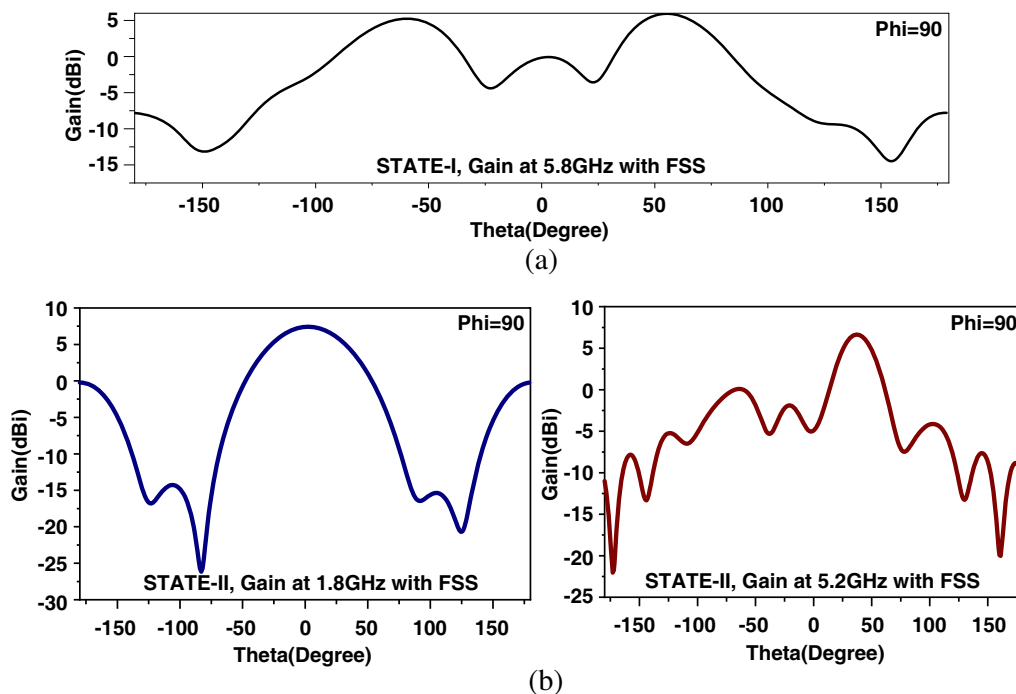


Figure 19. Gain versus elevation angle theta (Degree) with constant azimuth angle ($\phi = 90$ Degree) for (a) STATE-I, (b) STATE-II.

7. CONCLUSION

This paper presents a dual band reconfigurable antenna with a multilayer FSS reflector to improve the gain across all operating bands. The proposed antenna operates in one single-band and one dual-band mode and used for WLAN and GPS/RADAR applications. A significant enhancement in gain, around 5–6 dBi has been achieved in a low-profile design with a multilayer frequency selective surface (FSS) reflector. Compared to a single-band antenna, the proposed work offers additional antenna capability with a single PIN diode at a cheaper cost and in a substantially smaller size and space. The proposed antenna with FSS prototype model was built, and good agreement between simulated and experimental results was seen. As a consequence, the proposed antenna is beneficial for WLAN, RADAR, and other wireless technologies as well as being suitable for the integration in portable electronic devices.

ACKNOWLEDGMENT

The authors would like to thank The Science and Engineering Research Board (SERB), Department of Science and Technology, Government of India, for their assistance and support with this work (Grant File No. EMR/2016/007229/EEC).

REFERENCES

1. Shah, I. A., S. Hayat, A. Basir, M. Zada, S. A. A. Shah, and S. Ullah, "Design and analysis of a hexa-band frequency reconfigurable antenna for wireless communication," *AEU-International Journal of Electronics and Communications*, Vol. 98, 80–88, 2019.
2. Ullah, S., S. Ahmad, B. A. Khan, U. Ali, F. A. Tahir, and S. Bashir, "Design and analysis of a hexa-band frequency reconfigurable monopole antenna," *IETE Journal of Research*, Vol. 64, No. 1, 59–66, 2018.
3. Shah, I. A., S. Hayat, I. Khan, I. Alam, S. Ullah, and A. Afridi, "A compact, tri-band and 9-shape reconfigurable antenna for WiFi, WiMAX and WLAN applications," *International Journal of Wireless and Microwave Technologies (IJWMT)*, Vol. 6, No. 5, 45–53, 2016.
4. Kuo, Y. L. and K. L. Wong, "Printed double-T monopole antenna for 2.4/5.2 GHz dual-band WLAN operations," *IEEE Transactions on Antennas and Propagation*, Vol. 51, No. 9, 2187–2192, 2003.
5. Saleh, A. A. and A. S. Abdullah, "A novel design of patch antenna loaded with complementary split-ring resonator and L-shape slot for (WiMAX/WLAN) applications," *International Journal of Wireless and Microwave Technologies (IJWMT)*, Vol. 3, 16–25, 2014.
6. Park, Y. K. and Y. Sung, "A reconfigurable antenna for quad-band mobile handset applications," *IEEE Transactions on Antennas and Propagation*, Vol. 60, No. 6, 3003–3006, 2012.
7. Hayat, S., I. A. Shah, I. Khan, I. Alam, S. Ullah, and A. Basir, "Design of tetra-band frequency reconfigurable antenna for portable wireless applications," *2016 International Conference on Intelligent Systems Engineering (ICISE)*, 10–13, IEEE, January 2016.
8. Iddi, H. U., M. R. Kamarudin, T. A. Rahman, and R. Dewan, "Design of dual-band B-shaped monopole antenna for MIMO application," *Proceedings of the 2012 IEEE International Symposium on Antennas and Propagation*, 1–2, IEEE, July 2012.
9. Jing, S., Y. Yin, A. Sun, Y. Wei, and Y. Yang, "Compact E-shaped monopole antenna for dual-band WLAN applications," *2011 IEEE International Conference on Microwave Technology & Computational Electromagnetics*, 305–308, IEEE, May 2011.
10. Panda, J. R. and R. S. Kshetrimayum, "A printed F-shaped dual-band monopole antenna for RFID and WLAN applications," *2010 International Conference on Computer and Communication Technology (ICCT)*, 789–791, IEEE, September 2010.
11. Song, Y., Y. C. Jiao, H. Zhao, Z. Zhang, Z. B. Weng, and F. S. Zhang, "Compact printed monopole antenna for multiband WLAN applications," *Microwave and Optical Technology Letters*, Vol. 50, No. 2, 365–367, 2008.
12. Chang, T. H. and J. F. Kiang, "Compact multi-band H-shaped slot antenna," *IEEE Transactions on Antennas and Propagation*, Vol. 61, No. 8, 4345–4349, 2013.
13. Mahlaoui, Z., E. Antonino-Daviu, A. Latif, and M. Ferrando-Bataller, "Design of a dual-band frequency reconfigurable patch antenna based on characteristic modes," *International Journal of Antennas and Propagation*, Vol. 2019, Article ID 4512532, 12 pages, 2019.
14. Pandhare, R. A. and M. P. Abegaonkar, "Inset-feed frequency reconfigurable compact E-shape patch with DGS," *Progress In Electromagnetics Research C*, Vol. 101, 119–132, 2020.
15. Younus, K. M. and K. H. Sayidmarie, "A tri-band frequency reconfigurable slot antenna for wireless applications," *The Applied Computational Electromagnetics Society Journal (ACES)*, Vol. 35, 194–200, 2020.

16. Ellusamy, S. and R. Balasubramanian, "Sub-6 GHz quad-band reconfigurable antenna for 5G cognitive radio applications," *The Applied Computational Electromagnetics Society Journal (ACES)*, Vol. 36, No. 8, 1015–1025, 2021.
17. Pandhare, R. A., M. P. Abegaonkar, and C. Dhote, "UWB antenna with novel FSS reflector for the enhancement of the gain and bandwidth," *International Journal of Microwave and Wireless Technologies*, 1–16, 2022.
18. <https://www.macom.com/products/product-detail/MA4SPS402>.
19. Marcuiz, N., *Waveguide Handbook*, 1st Edition, McGraw-Hill, New York, 1951.
20. Segundo, F. C., A. L. P. Campos, A. Gomes Neto, and M. D. O. Alencar, "Double layer frequency selective surface for ultra wide band applications with angular stability and polarization independence," *Journal of Microwaves, Optoelectronics and Electromagnetic Applications*, Vol. 18, No. 3, 328–342, 2019.
21. Khalid, N. K. B. A. and F. B. C. Seman, "Double square loop frequency selective surface (FSS) for GSM shielding," *Advanced Computer and Communication Engineering Technology*, Vol. 315, 223–229, Springer, Cham, 2015.
22. Kushwaha, N. and R. Kumar, "High gain UWB antenna using compact multilayer FSS," *2014 IEEE International Microwave and RF Conference (IMaRC)*, 100–103, IEEE, December 2014.
23. Pandhare, R., M. Abegaonkar, and C. Dhote, "High gain wideband and multi-band on-demand reconfigurable antenna for modern wireless application," *International Journal of Microwave and Wireless Technologies*, 1–16, 2022, doi: 10.1017/S1759078722000630.